Archives of Biochemistry and Biophysics 771 (2025) 110513

Contents lists available at ScienceDirect

Archives of Biochemistry and Biophysics

journal homepage: www.elsevier.com/locate/yabbi

Organosilicon molecules bind to the intrinsically disordered protein NUPR1 by clamping its hot-spots

Laura F. Peña [h,1,2], Matías Estaras [a,1], Paula González-Andrés [h], Carlos Díez-Poza [h], Bruno Rizzuti [b,c], Olga Abian [c,d,e,f], Adrian Velazquez-Campoy [c,d,e,f], Juan L. Iovanna [a], Patricia Santofimia-Castaño [a], José L. Neira [c,g,*], Asunción Barbero [h,**]

[a] Centre de Recherche en Cancérologie de Marseille (CRCM), INSERM U1068, CNRS UMR 7258, Aix-Marseille Université and Institut Paoli-Calmettes, Parc Scientifique et Technologique de Luminy, 13288, Marseille, France
[b] CNR-NANOTEC, SS Rende (CS), Department of Physics, University of Calabria, Rende, 87036, Italy
[c] Instituto de Biocomputación y Física de Sistemas Complejos (BIFI), 50018, Zaragoza, Spain
[d] Instituto de Investigación Sanitaria Aragón (IIS Aragon), 50009, Zaragoza, Spain
[e] Centro de Investigación Biomédica en Red en el Área Temática de Enfermedades Hepáticas y Digestivas (CIBERehd), 28029, Madrid, Spain
[f] Departamento de Bioquímica y Biología Molecular y Celular, Universidad de Zaragoza, 50009, Zaragoza, Spain
[g] IDIBE, Universidad Miguel Hernández, 03202, Elche (Alicante), Spain
[h] Departamento Química Orgánica, Facultad de Ciencias (Campus Miguel Delibes), Universidad de Valladolid, Paseo de Belén 7, 47011, Valladolid, Spain

ARTICLE INFO

Keywords:
Organosilanes
Intrinsically disordered proteins
Protein-protein interactions
Organic synthesis

ABSTRACT

The nuclear protein 1, or NUPR1, is an intrinsically disordered protein (IDP) involved in the development and progression of pancreatic ductal adenocarcinoma (PDAC). We have previously developed drugs capable of binding at the two hot-spot regions of NUPR1, around residues Ala33 and Thr68, hampering its interactions *in cellulo*. In this work, we synthesized new organosilicon molecules targeting those key hot-spots. The compounds were obtained by an acid-catalyzed intramolecular cyclization of a starting alkenol that contains a silyl group attached to the double bond. Binding between the silyl compounds and NUPR1 involved the two hot-spots, as shown by 2D ^{1}H–^{15}N HSQC NMR. Molecular simulations clarified that the binding relies on a loose clamp mechanism of the ligands towards the hot-spots. The dissociation constants (K_d) were around 20 μM, as measured by several biophysical techniques. However, studies *in cellulo* with PDAC cells did not show a decrease of cell viability upon treatment with the compounds; furthermore, proximity ligation assays *in cellulo* with a natural partner protein of NUPR1, G3BP, did not show a significant level of interfering in such interaction when silyl compounds were present, probably due to the high hydrophobicity of the designed compounds. Thus, in the case of NUPR1, moderate-to-high drug binding affinities (K_d < 10 μM) *in vitro* and a higher hydrophilicity are necessary to hamper protein-protein interactions *in cellulo*. As a more general conclusion, *in vitro* binding of ligands to the protein hot-spots is a necessary condition in the drug design targeting IDPs, but it is not enough to guarantee inhibition of their interactions *in cellulo*.

Abbreviations: aq., aqueous; BLI, biolayer interferometry; BPO, benzoyl peroxide; calc., calculated; DMSO, di-methyl sulfoxide; equiv., equivalent(s); ESI, electrospray ionization; G3BP, Ras-GTPase-activating protein (SH3 domain)-binding protein; HMBC, heteronuclear multiple-bond correlation; HMRS, high resolution mass spectrometry; HSQC, heteronuclear single-quantum coherence; IDP, intrinsically disordered protein; ITC, isothermal titration calorimetry; M.p., melting point; NMR, nuclear magnetic resonance; NBS, *N*-bromosuccinimide; NOE, nuclear Overhauser effect; NUPR1, nuclear protein 1; OTMS, octadecyltrimethoxysilane; PDAC, pancreatic ductal adenocarcinoma; PLA, proximity ligation assay; PPI, protein-protein interaction; sat., saturated; TFP, trifluoperazine; THF, tetrahydrofuran; TLC, thin-layer chromatography; TMSBr, trimethylsilyl bromide; TMSCl, trimethylsilyl chloride; TMSOTf, trimethylsilyl trifluoromethanesulfonate; TOF, time-of-flight; TPPI, time proportional phase increment; TSP, 3-(trimethylsilyl)propionic-2,2,3,3-d_4 acid sodium salt; UPLC-MS, ultra-performance liquid chromatography-mass spectrometry.

* Corresponding author. Universidad Miguel Hernández, Avda. del Ferrocarril s/n, 03202, Elche (Alicante), Spain.
** Corresponding author. Departamento Química Orgánica, Facultad de Ciencias (Campus Miguel Delibes), Universidad de Valladolid, Paseo de Belén 7, 47011, Valladolid, Spain.
E-mail addresses: jlneira@umh.es (J.L. Neira), asuncion.barbero@uva.es (A. Barbero).
[1] These authors contributed equally to this work.
[2] Current address: Departamento Química Orgánica, University of Castilla-La Mancha, Faculty of Pharmacy, Calle Almansa 14, Edif. Bioincubadora, 02008, Albacete, Spain

https://doi.org/10.1016/j.abb.2025.110513
Received 7 May 2025; Received in revised form 14 June 2025; Accepted 16 June 2025
Available online 19 June 2025

1. Introduction

The nuclear protein 1 (NUPR1) is an 82-residue-long, intrinsically disordered protein (IDP) having key roles in cellular stress, ranging from being a transcription factor to a regulator of apoptosis [1–4], and it is involved in interactions with different natural partners, from proteins to carbohydrates and nucleic acids [4–7]. NUPR1 is specifically overexpressed in pancreatic ductal adenocarcinoma (PDAC), compared to its negligible expression in normal tissues. In fact, NUPR1 intervenes in the incidence, development and metastasis of PDAC [1,2,8], and it can be considered as a potential therapeutic target for this serious illness [9,10]. Due to its intrinsically disordered nature, finding inhibitors targeting NUPR1 poses significant challenges to traditional drug design, because conventional structure-based approaches cannot be used. To overcome these challenges, we have previously employed a mid-throughput experimental screening to repurpose the antipsychotic drug trifluoperazine (TFP) as a NUPR1 inhibitor [11]. TFP has been improved *in silico* by computer modelling, and the synthesis of several new compounds, together with the use of an array of biological, biochemical and biophysical methods, has led to the development of ZZW-115, an inhibitor of NUPR1 protein-protein interactions (PPIs), resulting in the suppression of tumor cell growth both *in cellulo* and *in vivo* [12,13]. However, as a TFP analog, ZZW-115 has cardiotoxic side effects, which makes it necessary to find or develop new NUPR1 inhibitors [14].

The design of drugs for disease treatment requires not only minimal (or complete lack of) toxicity, but also high activity, solubility and selectivity, and a physiologically acceptable pharmacokinetics. Drug developers usually focus on well-established families of compounds to simplify and accelerate the design of new active compounds. In fact, around a few dozen scaffolds are routinely used in new drug design, with only a limited number of functional groups repeatedly utilized in their development [15,16]. The steric patterns available for organosilicon compounds, combined with the substitution of carbon by silicon, open the road to new opportunities in the design and control of stability, toxicity, solubility, and physiologically acceptable pharmacokinetic properties of innovative drugs. Thus, strategic incorporation of silicon bio-isosteres into well-known drug scaffolds is a strategy to enhance the therapeutic potential of a drug or, alternatively, to drug repurposing. Generally, silicon-containing compounds are more lipophilic (and therefore, more hydrophobic) than their corresponding carbon counterparts. Modulating the lipophilicity of a molecule can result in the modification of its *in vivo* effects and pharmacological properties; for instance, an increase in a compound lipophilicity enhances its ability to penetrate membranes and cross the blood-brain barrier [17,18]. In addition, silicon-containing molecules are less prone to hepatic metabolism, resulting in a longer half-life of these compounds when compared to their carbon counterparts [17]. At the same time, the presence of quaternary carbons in natural products has been shown to significantly enhance their selectivity and efficiency in binding to target proteins, particularly when compared to planar, sp^2-rich compounds [19].

In this work, we have selected molecular models that incorporate both complementary structural features – a silicon atom bearing bulky ligands and a quaternary carbon with electronically diverse substituents – to investigate their interactions with NUPR1, namely, we have synthesized organosilicon molecules with silicon in the central position, surrounded by bulky ligand moieties. We have tested the binding of organosilicon molecules to NUPR1, by using various biophysical and spectroscopic probes, namely isothermal titration calorimetry (ITC), nuclear magnetic resonance (NMR), and biolayer interferometry (BLI). As shown by ITC (the gold standard technique for determining affinity measurements) these molecules interacted with NUPR1 with an affinity around 20 μM. Association of these compounds to NUPR1 was also confirmed by BLI. Furthermore, we demonstrated that the binding region comprised the two hot-spots of NUPR1: the regions around Ala33 and Thr68 in its sequence, by using 2D $^{1}H,^{15}N$-HSQC NMR, which showed chemical shift changes and/or signal broadening at several cross-peaks around those residues. Molecular docking simulations provided also a description of the binding mechanism of the silyl compounds at atomic level, based on a clamp of the fuzzy ensemble of local conformations of the hot-spot regions of NUPR1. However, proximity ligation assays (PLAs) and viability studies *in cellulo* in the presence of these organosilicons did not show any hampering of the PPIs that involved NUPR1. Then, we could conclude that the involvement of hot-spots is a prerequisite for binding of drugs to IDPs, but it may not be enough to achieve effective inhibition of such pharmacological IDP target *in cellulo* if: (i) the affinity constant is above a specific range (in the case of NUPR1, a dissociation constant lower than 20 μM seemed to be required); and/or (ii) hydrophobicity of the compounds is very high.

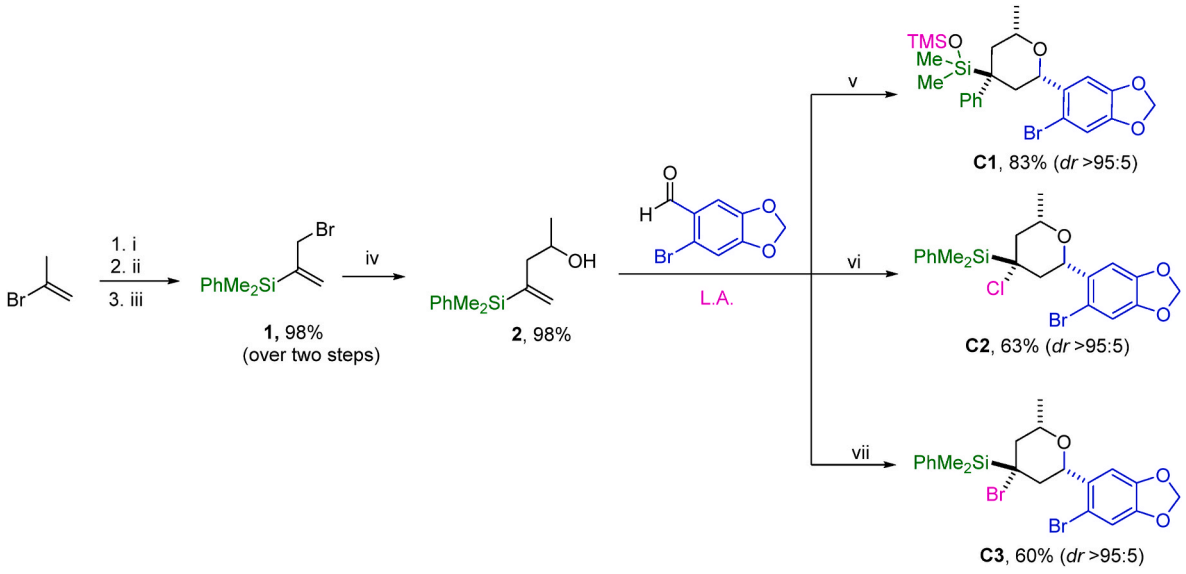

SCHEME 1. Synthesis of the organosilicon compounds **C1**, **C2** and **C3**. Reagents and conditions: (i) Mg, dry THF, 50 °C, 30 min; (ii) $PhMe_2SiCl$, reflux, 2 h; (iii) NBS, BPO, dry hexane, reflux, 4 h; (iv) Zn, CH_3CHO, NH_4Cl/THF (1:0.2), at room temperature, 3 h; (v) 6-bromopiperonal, TMSOTf, dry CH_2Cl_2, – 78 °C, 1 h; (vi) 6-bromopiperonal, $BiCl_3$, TMSCl, dry CH_2Cl_2, 0 °C, 1 h; (vii) 6-bromopiperonal, TMSBr, dry CH_2Cl_2, -78 °C, 1 h. The different colors indicate the different substituents added at the different synthetic steps to the silicon scaffold (the color code is the same as in Fig. 1).

Furthermore, based on our results *in vitro*, we also conclude that organosilicon compounds can be designed to target IDPs.

2. Materials and methods

2.1. Materials

Imidazole, Trizma acid and its base, NaCl, di-methyl sulfoxide (DMSO), protease inhibitor tablets EDTA-free, Ni^{2+}-resin, TSP and Amicon centrifugal devices with a molecular weight cut-off of 3 kDa were from Merck (Madrid, Spain). Kanamycin, ampicillin and isopropyl-β-D-1-thiogalactopyranoside (IPTG) were obtained from Apollo Scientific (Stockport, UK). Triton X-100, and the sodium-dodecyl-sulfate (SDS) protein marker (PAGEmark Tricolor) were from VWR (Barcelona, Spain). The rest of the materials were of analytical grade. Water was deionized and purified on a Millipore system.

All chemicals employed in the synthesis of the organosilicon molecules were purchased from CymitQuimica (Barcelona, Spain) or Sigma-Aldrich (Madrid, Spain). Unless otherwise noted, experiments were carried out with dry solvents under nitrogen atmosphere. Dichloromethane was dried with pre-activated molecular sieves. Flash column chromatography was performed using Silica Gel 60 (230–400 mesh American Society for Testing and Materials (ASTM)). Thin layer chromatography (TLC) was performed using aluminium backed plate, pre-coated with silica gel (0.20 mm, silica gel 60) with a fluorescent indicator (254 nm) from Macherey-Nagel (Dueren, Germany).

2.2. Chemistry

Silylated compounds, **C1–C3,** were obtained in a four-step reaction sequence, as depicted in Scheme 1. The key intermediate of this process is vinylsilyl alcohol **2** (Scheme 1), which is readily prepared in three steps starting from commercially available materials. All three compounds **C1–C3** feature a silyl group with bulky substituents, as well as a distinct quaternary carbon at the C-4 position of the tetrahydropyran unit. The synthesis of the starting alcohol **2** has been already described [20].

2.2.1. TMSOTf-promoted cyclization of vinylsilyl alcohol *2* to obtain *C1*

A solution of 100 mg of the alcohol **2** (0.45 mmol) and 115 mg of 6-bromopiperonal (0.50 mmol, 1.1 equiv.) in 4.5 mL of dry dichloromethane was cooled to – 78 °C (under nitrogen). Then, 0.12 mL (0.68 mmol, 1.5 equiv.) was added dropwise. Finally, the mixture was stirred for 1 h while it was monitored by TLC. When starting materials were consumed, it was hydrolyzed with 4.5 mL of NaOH (aq.) 2 M. Phases were then separated, and the aqueous phase was extracted three times with dichloromethane (3 × 10 mL). The organic phases were combined, washed with NaCl sat. (20 mL) and dried over anhydrous $MgSO_4$; the solvent was evaporated under reduced pressure. The crude mixture was analyzed by NMR, and purified by column chromatography in silica gel, using a 30:1 mixture of hexane-ethyl acetate, yielding compound **C1** as a white solid (196 mg, 83 %). M.p. = 83.1–88.8 °C. Spectroscopic data for 1-((2*S**,4*S**,6*S**)-2-(6-bromobenzo[*d*] [1,3]dioxol-5-yl)-6-methyl-4--phenyltetrahydro-2*H*-pyran-4-yl)-1,1,3,3,3-pentamethyldisiloxane (**C1**) are: ^{1}H NMR (500 MHz, $CDCl_3$) *δ* 7.41–7.29 (m, 4H, Ar–*H*), 7.17–7.11 (m, 2H, Ar–*H*), 6.95 (s, 1H. Ar–*H*), 6.00–5.91 (m, 2H, O–C*H*$_2$–O), 4.73 (dd, *J* = 11.0, 2.0 Hz, 1H, O–C*H*), 3.81–3.72 (m, 1H, *H*C-O), 2.46 (dt, *J* = 14.3, 2.0 Hz, 1H, C*H*H), 2.29 (dt, *J* = 14.2, 1.9 Hz, 1H, C*H*H), 1.70 (dd, *J* = 14.2, 10.9 Hz, 1H, CH*H*), 1.62 (dd, *J* = 14.3, 11.0 Hz, 1H, CH*H*), 1.23 (d, *J* = 6.1 Hz, 3H, CH_3), 0.01 (s, 9H, $(CH_3)_3$–Si), −0.10 (s, 3H, (CH_3–Si), −0.11 (s, 3H, (CH_3–Si). ^{13}C NMR (101 MHz, $CDCl_3$) *δ* 147.9 (C), 147.4 (C), 142.0 (C), 136.8 (C), 128.3 (CH), 128.0 (CH), 124.5 (CH), 112.4 (CH), 111.6 (C), 107.9 (CH), 101.8 (CH_2), 74.2 (CH), 68.9 (CH), 36.5 (CH_2), 36.1 (CH_2), 34.7 (C), 22.4 (CH_3), 2.0 (CH_3), −3.1 (CH_3), −3.1 (CH_3). HRMS (ESI^+) *m/z* (mass to charge ratio) calc. for $C_{24}H_{33}BrO_4Si_2Na$ ([M + Na]$^+$): 543.0993, found 543.1011.

The UV absorbance spectrum of the compound showed a maximum at 295 nm.

The spectroscopic material and NMR and HRMS data are provided in Fig. S1.

2.2.2. TMSCl/$BiCl_3$-promoted cyclization of vinylsilyl alcohols *2* to obtain *C2*

A solution of 7.1 mg of $BiCl_3$ (0.023 mmol, 0.05 equiv.) and 124 mg of 6-bromopiperonal (0.54 mmol,1.2 equiv.) in 4.5 mL of dry dichloromethane was cooled to 0 °C (under nitrogen). Then, the corresponding Lewis acid, TMSCl (0.068 mL, 0.54 mmol, 1.2 equiv.), was added dropwise. The mixture was stirred for 5 min and 100 mg of the alcohol **2** (0.45 mmol, 1.0 equiv.) were dissolved in 0.2 mL of dry dichloromethane and added dropwise into the reaction. The mixture was stirred at 0 °C while monitored by TLC. When starting materials were consumed, it was hydrolyzed with 5 mL of $NaHCO_3$ (sat.). Phases were then separated, extracting the aqueous phase three times with dichloromethane (3 × 10 mL). The organic phases were combined, washed with NaCl sat. (20 mL) and dried over anhydrous $MgSO_4$. The solvent was then evaporated under reduced pressure. The crude mixture was analyzed by NMR and then purified by column chromatography in silica gel, using a 30:1 mixture of hexane-ethyl acetate, yielding compound **C2** as a white solid (134 mg, 63 %). M.p. = 105.6–107.7 °C. Spectroscopic data for (2*S**,4*R**,6*S**)-2-(6-bromobenzo[*d*] [1,3]dioxol-5-yl)-4-chloro-6-methyltetrahydro-2*H*-pyran-4-yl)dimethyl(phenyl) silane (**C2**) are: ^{1}H NMR (500 MHz, $CDCl_3$) *δ* 7.72–7.68 (m, 2H, Ar–*H*), 7.43–7.35 (m, 3H, Ar–*H*), 7.04 (s, 1H, Ar–*H*), 6.93 (s, 1H, Ar–*H*), 5.95–5.93 (m, 2H, O–C*H*$_2$–O), 4.63 (dd, *J* = 11.9, 2.0 Hz, 1H, O–C*H*), 3.60–3.51 (m, 1H, *H*C-O), 2.62 (dt, *J* = 13.5, 2.0 Hz, 1, C*H*H), 2.36 (dt, *J* = 13.4, 1.9 Hz, 1H, C*H*H), 1.84 (dd, *J* = 13.4, 11.6 Hz, 1H, CH*H*), 1.79 (dd, *J* = 13.5, 11.9 Hz, 1H, CH*H*), 1.18 (d, *J* = 6.1 Hz, 3H, CH_3), 0.66 (s, 3H, CH_3–Si), 0.62 (s, 3H, CH_3–Si). ^{13}C NMR (101 MHz, $CDCl_3$) *δ* 147.9 (C), 147.8 (C), 136.3 (C), 135.2 (CH), 135.1 (CH), 129.9 (CH), 128.0 (CH), 112.3 (CH), 111.7 (C), 107.7 (CH), 101.9 (CH_2), 76.2 (CH), 71.5 (CH), 60.7 (C), 46.7 (CH_2), 45.8 (CH_2), 22.2 (CH_3), −2.5 (CH_3), −2.6 (CH_3). HRMS (ESI^+) *m/z* calc. for $C_{21}BrClH_{24}NaO_3Si$ ([M + Na]$^+$): 489.0259, found 489.0266.

The UV absorbance spectrum of the compound showed a maximum at 295 nm.

The spectroscopic material and NMR and HRMS data are provided in Fig. S1.

2.2.3. TMSBr-promoted cyclization of vinylsilyl alcohol *2* to obtain *C3*

A solution 6-bromopiperonal (1.2 equiv.) in dry dichloromethane (0.1 M) was cooled to −78 °C (under nitrogen). Then, the corresponding Lewis acid, TMSBr (1.2 equiv.), was added dropwise. The mixture was stirred for 5 min and the corresponding alcohol **2** (100 mg, 1.0 equiv.) was dissolved in 0.2 mL of dry dichloromethane and added dropwise into the reaction. The mixture was stirred at – 78 °C while monitored by TLC. When starting materials were consumed, it was hydrolyzed with 5 mL of $NaHCO_3$ (sat.). Phases were then separated, extracting the aqueous phase three times with dichloromethane (3 × 10 mL). The organic phases were combined, washed with NaCl sat. (20 mL) and dried over anhydrous $MgSO_4$. The solvent was then evaporated under reduced pressure. The crude mixture was analyzed by NMR and then purified by column chromatography in silica gel, using a 30:1 mixture of hexane-ethyl acetate, yielding compound **C3** as a white solid (134 mg, 63 %). M.p. = 121.4–123.9 °C. Spectroscopic data for (2*S**,4*R**,6*S**)-2-(6-bromobenzo[*d*] [1,3]dioxol-5-yl)-4-bromo-4-(dimethyl(phenyl)silyl)-6 -methyltetrahydro-2*H*-pyran (**C3**) are: ^{1}H NMR (500 MHz, $CDCl_3$) *δ* 7.74–7.70 (m, 2H, Ar–*H*), 7.43–7.36 (m, 3H, Ar–*H*), 7.05 (s, 1H, Ar–*H*), 6.93 (s, 1H, Ar–*H*), 5.95 (s, 2H, O–CH_2–O), 4.62 (dd, *J* = 11.6, 2.1 Hz, 1H, O–C*H*), 3.58–3.51 (m, 1H, *H*C-O), 2.79 (dt, *J* = 13.5, 1.9 Hz, 1H, C*H*H), 2.52 (dt, *J* = 13.4, 1.8 Hz, 1H, C*H*H), 2.14 (dd, *J* = 13.4, 11.5 Hz, 1H, CH*H*), 2.10 (dd, *J* = 13.5, 11.6 Hz, 1H, CH*H*), 1.17 (d, *J* = 6.1 Hz, 3H, CH_3), 0.70 (s, 3H, CH_3–Si), 0.67 (s, 3H, CH_3–Si). ^{13}C NMR (101

MHz, $CDCl_3$) δ 147.9 (C), 147.8 (C), 136.8 (CH), 135.2 (C), 135.0 (C), 129.9 (CH), 128.0 (CH), 112.3 (CH), 111.6 (C), 107.7 (CH), 101.9 (CH_2), 76.7 (CH), 72.1 (CH), 58.2 (C), 47.5 (CH_2), 46.7 (CH_2), 22.1 (CH_3), −1.3 (CH_3), −1.9 (CH_3). HRMS (ESI+) *m/z* calc. for $C_{21}H_{24}Br_2NaO_3Si$ ($[M + Na]^+$): 532.9769, found 532.9754.

The UV absorbance spectrum of the compound showed a maximum at 295 nm.

The spectroscopic material and NMR and HRMS data are provided in Fig. S1.

2.3. Protein expression and its purification, and preparation of the organosilicon compound stock solutions

NUPR1 was produced and purified from transformed BL21 (DE3) *E. coli* strain (Merck, Madrid, Spain) grown in Luria-Bertani broth medium as previously described [4]. For the ^{15}N-labeled NUPR1 the procedure was the same as in rich medium, by using minimal medium and 1 g/L of $^{15}NH_4Cl$ [7,21]. The NUPR1 concentrations were obtained from the absorbance measurement at 280 nm, by using the values for model compounds [22], and considering the presence of two tyrosines in its sequence.

The stock solutions of the compounds used for the *in vitro* and *in cellulo* experiments were prepared by dissolving an amount between 27 and 58 mg of the corresponding organosilicon in DMSO (usually in a volume of 1–2 mL to yield stock solutions of 50–60 mM). Diluted working solutions were prepared from these stock solutions to carry out the titrations in the BLI or ITC experiments. Although we did not observe any deviation to the Lambert-Beer law in the concentration range explored (section 2.4), we suspect that the compounds had a tendency to self-associate, as, given their small molecular weight, we were able to measure their binding to NUPR1 by using BLI (section 2.8.).

2.4. Ultraviolet absorbance (UV)

All absorption spectra were recorded between 400 and 200 nm on an UV–Visible spectrophotometer UV-1603 by Shimadzu (Kyoto, Japan). All spectra were acquired at room temperature. DMSO was used as a reference for a blank subtraction for all the analyzed samples at the different compound concentrations.

To determine the molar extinction coefficient of each compound, the absorbance at different concentrations of the corresponding compound was measured at 295 nm, where all the silicon compounds showed a maximum (Fig. S1). The range of explored concentrations was 19–160 μM in DMSO solutions. Fitting of the absorbance to the Lambert-Beer law was carried out by using KaleidaGraph (Synergy Software, Reading, PA, USA). We did not observe any deviation to the Lambert-Beer law in such explored concentration range, that is, in that concentration range, we observed a straight line.

2.5. Nuclear magnetic resonance (NMR)

The NMR experiments for the interaction between silyl compounds and NUPR1 were performed at 25 °C, pH 4.5 (acetate buffer), on a Bruker Avance II DRX-500 spectrometer (Bruker, Karlsruhe, Germany) equipped with a triple-resonance probe and z gradients. Spectra were acquired at such pH because under this condition assignment has been already carried out, and a larger number of cross-peaks can be observed, as the hydrogen-exchange is decreased. All spectra were referenced to external TSP, as previously described [5,7]. The 2D ^1H,^{15}N-heteronuclear single-quantum coherence (HSQC) spectra were acquired either for isolated ^{15}N-labeled NUPR1 (80 μM), in the presence of a concentration of 0.4 % (v/v) of DMSO, or alternatively, in the presence of the corresponding selected organosilicon compound (300 μM), which resulted in a final concentration of 0.4 % (v/v) DMSO in the solution. Frequency discrimination in the indirect dimensions was achieved by using the echo/antiecho-TPPI method. The spectra were acquired with 1024 points in the ^1H dimension, 128 points in the ^{15}N dimension, and 200 scans. The carrier of the ^1H dimension was set at 5.00 ppm, and that of ^{15}N was set at 120 ppm. The spectral widths used were 10 ppm and 35 ppm in the ^1H and ^{15}N dimensions, respectively. Water signal was suppressed with the WATERGATE sequence [23]. Data were zero-filled to double the number of original points in both dimensions, apodized with shifted squared sine-bell functions in the two dimensions, and Fourier transformed with the program TopSpin 2.1 (Bruker, Karlsruhe, Germany). Assignments for every amide proton and ^{15}N nucleus were taken from those previously reported for isolated NUPR1 in water at the same pH and temperature [5].

NMR spectra used for the identification and characterization of silyl compounds were recorded at the Laboratory of Instrumental Techniques (L.T.I., www.laboratoriotecnicasinstrumentales.es, University of Valladolid), by using either a Varian 400 MHz (^1H, 399.85 MHz; ^{13}C, 100.6 MHz) or a Varian 500 MHz spectrometer (^1H, 500.12 MHz; ^{13}C, 126 MHz), at room temperature (25 °C). Chemical shifts (δ) were reported in parts per million (ppm) relative to the residual solvent peaks recorded, rounded to the nearest 0.01 ppm for ^1H NMR and 0.1 ppm for ^{13}C NMR (reference: $CDCl_3$ [^1H: 7.26, ^{13}C: 77.2]). Spin-spin coupling constants (J) in ^1H NMR were given in Hz and rounded to the nearest 0.1 Hz, and peak multiplicity was indicated as follows: s (singlet), d (doublet), t (triplet), q (quartet), m (multiplet) and br (broad). ^{13}C NMR were recorded with complete proton decoupling. Carbon types, structure assignments and attribution of peaks were determined from two-dimensional correlation experiments (HSQC, correlation spectroscopy (COSY) and heteronuclear multiple-bond correlation (HMBC)). Relative stereochemistry was assigned based on the 2D-NOE experiments.

2.6. High-resolution mass spectrometry

High-resolution mass spectra (HRMS) were measured at the mass spectrometry service of the Laboratory of Instrumental Techniques, University of Valladolid, using a quadrupole spectrometer equipped with a TOF analyzer, on a UPLC-MS system (UPLC: Waters ACQUITY H-class UPLC; MS: Bruker Maxis Impact) by positive electrospray ionization (ESI^+).

2.7. Isothermal titration calorimetry (ITC)

The interaction of NUPR1 with the organosilicon compounds was assessed by using an automated Auto-iTC200 high-sensitivity calorimeter (MicroCal, Malvern-Panalytical, Malvern, UK). To avoid issues related to bubble formation in the cell and syringe, and to ensure a good quality of the assays, both the protein and the organosilicon compounds were degassed. Experiments were performed at 25 °C in buffer 50 mM Tris, pH 7.5, 17 % (v/v) DMSO; under these conditions, NUPR1 remained disordered (unpublished results) as judged by 2D ^1H,^{15}N-HSQC spectra, and we did not observe any dilution effect (i.e., variable injection heats) of the compounds when control experiments were carried out by injecting the corresponding organosilicon compound, **Cx**, against buffer. The silyl compounds (100 μM, in the injection syringe) were titrated into NUPR1 (10 μM, in the calorimetric cell). A series of 19 injections with 2 μL volume, 0.5 μL/s injection speed, and 150 s time spacing was programmed while maintaining a reference power of 10 μcal/s and a stirring speed of 750 rpm. The interaction isotherm was generated by plotting the ligand-normalized heat effect per injection, calculated by integration of the thermogram raw data (thermal power as a function of time) after baseline correction, as a function of the molar ratio ($[\mathbf{Cx}]_T/[NUPR1]_T$) [24]. The isotherm was analyzed through non-linear least-squares regression data analysis, applying a model that considers a single binding site. Fitting provided estimates for the association constant, K_a, the interaction enthalpy, ΔH, and the apparent stoichiometry of binding n (although, in practice, this last parameter usually reports the fraction of active protein in the sample within the calorimetric cell). The dissociation constant was calculated from the

association constant: $K_d = 1/K_a$. The background injection heat (usually called "dilution heat", reflecting any unspecific phenomenon such as titrant/solute dilution, buffer neutralization, temperature equilibration, or solution mechanical mixing) was accounted for by including an adjustable constant parameter in the fitting function. The data analysis was conducted in Origin 7.0 (OriginLab, Northampton, MA) with user-defined fitting functions.

2.8. Biolayer interferometry (BLI)

2.8.1. Experimental design of BLI experiments

The kinetic association (k_{on}) and dissociation (k_{off}) rate constants of the binding of the organosilicon compounds to NUPR1 were determined by using a BLItz system (ForteBio Pall, Barcelona, Spain) [25]. The buffer used in the experiments was that recommended by the manufacturer (Octet Kinetics buffer 10 ×). As NUPR1 had a His-tag, it was immobilized on His-tag biosensors (Forte Bio) at the concentration of 0.8 μM. The silyl compound concentration was varied in the range from 4 to 45 μM during the association step. The general schemes of the NUPR1/**Cx** association/dissociation reactions in the BLItz system were: 30 s of acquisition of the initial baseline with the 10 × kinetics buffer; 120 s of loading NUPR1 into the biosensor; 30 s of baseline acquisition with the 10 × kinetics buffer; 120 s of association of the silyl compound to the NUPR1-loaded biosensor; and 120 s of dissociation of the silyl compound from the biosensor.

2.8.2. Fitting of the sensorgrams

Fittings of the sensorgrams were carried out by using KaleidaGraph. The interferometry response during the association step (measured in response units, RU), $R(t)$, and the binding rate, $dR(t)/dt$, were used to evaluate the kinetics of the formation of the NUPR1/silyl compound complex, according to:

$$\frac{dR(t)}{dt} = k_{on}[Cx](R_{max} - R(t)) - k_{off}R(t) \quad (1)$$

where R_{max} is proportional to the total concentration of biosensor-bound NUPR1; and **[Cx]** represents the corresponding concentration of organosilicon molecules.

In Eq. (2), $R(t)$ is given by:

$$R(t) = R_{eq} - R_{eq}e^{(-k_{obs}\ (t-t_0))} \quad (2)$$

where R_{eq} is the steady-state (or equilibrium) response obtained at infinite time when $dR(t)/dt = 0$, and $t_0 = 180$ s is the time at which the association step between biosensor-immobilized NUPR1 and the organosilicon in the solution started. Since we observed a slope at the largest observation times, we fitted the experimentally obtained $R(t)$ under any condition as:

$$R(t) = R_{eq} - R_{eq}e^{(-k_{obs}\ (t-t_0))} - \acute{R}_{eq}(t - t_0) \quad (3)$$

The k_{obs} was used for the pseudo-first order plots, where its value is given by:

$$k_{obs} = k_{on}\ [Cx] + k_{off} \quad (4)$$

The dissociation process was always fitted to a single exponential, with $R(t)$ given by:

$$R(t) = R_1\ e^{(-k_{off}(t-t_0))} \quad (5)$$

where $t_0 = 300$ s is the time at which the dissociation of the silyl compound from the biosensor-bound NUPR1 started in our experimental set-up, and R_1 is the response level when dissociation started.

2.9. Flexible molecular docking

The association between each silyl compound and NUPR1 was studied by using molecular docking, with full flexibility for both the ligands and the protein fragments considered. The protocol followed was the same that we had already used for drug design studies against this IDP [12,13,26]. The three compounds were each considered in the simulations as a flexible host (with 5 rotatable bonds for compound **C1**, and 3 for both **C2** and **C3**), and the two hot-spot regions S^{31}LAHS^{35} and L^{66}VTKL^{70} of NUPR1 (with 18 and 22 rotatable bonds, respectively) were docked onto them. The protein fragments were acetylated and *N*-methylated at the two termini, respectively, to avoid the introduction of spurious charged groups at both ends.

All the molecular species were prepared by using the AutoDock Tools modeling software, version 1.5.6 [27], and included all non-hydrogen atoms and polar hydrogens. Simulations were performed using the AutoDock Vina docking engine, version 1.2.5 [28], which also includes parameters for silicon (atom type Si). A search volume of 30 Å × 30 Å × 30 Å was considered around each silyl compound, as the NUPR1 fragments in extended conformation are shorter than 25 Å. The ten most favorable docking poses were considered in the subsequent analysis.

2.10. Cell culture and viability tests

MiaPaCa cells were cultured in Dulbecco's modified Eagle's medium (DMEM) supplemented with 10 % fetal bovine serum (FBS) at 37 °C and 5 % CO_2.

For cell viability determination, the PrestoBlue™ reagent was used, following the manufacturer's instructions. Briefly, MiaPaCa cells were seeded in a 96-well plate at 5000 cells per well and allowed to adhere overnight. The next day, cells were treated with a range of organosilicon molecule concentrations (0.01–100 μM); for the most concentrated solution of the corresponding **Cx** compound, the final concentration of DMSO was 0.02 % (v/v)) and incubated for 72 h. Viability was assessed by adding PrestoBlue™ reagent for 2 h and results were normalized with respect to those obtained with untreated cells.

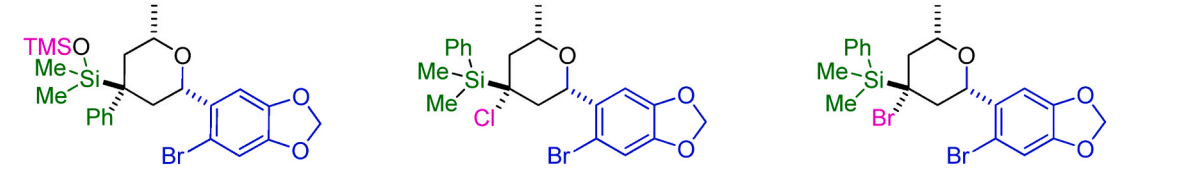

C1
Chemical Formula: $C_{24}H_{33}BrO_4Si_2$
Molecular Weight: 521,59 g/mol

C2
Chemical Formula: $C_{21}H_{24}BrClO_3Si$
Molecular Weight: 467,86 g/mol

C3
Chemical Formula: $C_{21}H_{24}Br_2O_3Si$
Molecular Weight: 512,31 g/mol

Fig. 1. Organosilicon molecules: Structures of the compounds of interest **C1**, **C2** and **C3**. The different colors indicate the different substituents added at the different synthetic steps to the silicon scaffold. (For interpretation of the references to color in this figure legend, the reader is referred to the Web version of this article.)

2.11. Proximity ligation assay (PLA)

MiaPaCa cells were seeded on coverslips with 100,000 cells and allowed to attach overnight. The next day, cells were treated with 100 μM (final 0.02 % (v/v) concentration of DMSO) of each organosilicon molecule for 3 or 6 h. Cells were then fixed with 4 % paraformaldehyde and permeabilized with 0.2 % Triton X-100. Immunostaining was performed by using Duolink In Situ (Merck) according to the manufacturer's protocol, with anti-NUPR1 (rabbit, homemade) and anti-G3BP (mouse, Abcam, ab56574) antibodies. Images were collected on a Zeiss Axio Imager Z2 microscope apotome (× 40 lens). Quantification of PLA dots per nuclei was calculated by ImageJ (Fiji) software.

3. Results

3.1. Versatile synthesis of the organosilicon compounds

As previously mentioned in section 1, we aimed to synthesize oxacyclic compounds incorporating two complementary structural features: (i) a silyl group, specifically organosilicon moieties bearing groups of varying size at the silicon centre (Fig. 1); and (ii) a quaternary carbon bearing different substituents. To assess how substituent size and electronic properties influence protein binding, we focused on a series of tetrahydropyran derivatives (**C1**–**C3**).

Compounds **C2** and **C3**, which feature a halogen atom (Cl or Br, respectively) at the C4 position of the oxane ring, were designed to probe how variation in size and electronic properties at this site influence binding affinity. In contrast, compound **C1**, bearing a phenyl group at C4 position, was chosen to investigate whether increased aromatic bulk and hydrophobicity enhance binding to the target protein. Additionally, **C1** also incorporates a trimethylsilyloxy (TMSO) group directly bonded to silicon, in place of the phenyl substituents used in **C2** and **C3**, with the aim of improving its solubility.

The synthetic route for preparing the desired silylated compounds **C1–C3** (Fig. 1) is illustrated in Scheme 1. The starting vinylsilyl alcohol **2** was readily prepared in three linear steps using a methodology developed in our laboratory. Thus, 3-bromo-2-(phenyldimethylsilyl) propene **1** was obtained in high yield by reaction of the Grignard reagent of 2-bromopropene with phenyldimethylsilylchloride, followed by allylic bromination of the resulting 2-(phenyldimethylsilyl)propene (carried out using *N*-bromosuccinimide as the bromide source). Finally, Barbier reaction of **1** (using an *in-situ* generated organozinc reagent in aqueous medium) provided alcohol **2**, which is the key intermediate required for the cyclization processes. Once alcohol **2** was synthesized, it was submitted to reaction with 6-bromopiperonal in the presence of different Lewis acids, in a so-called silyl-Prins cyclization. As we have previously reported [29], an intriguing 1,2-phenyl migration process from silicon to carbon was observed, whose occurrence was strongly influenced by the nature of the Lewis acid used. Thus, when trimethylsilyl trifluoromethanesulfonate (TMSOTf) was employed as the activator, the reaction yielded tetrahydropyranyl derivative **C1**, in which the silyl group remained in the molecule while the aryl group migrated from silicon to the adjacent quaternary carbon [29]. In contrast, the use of trimethylsilyl halides resulted in tetrahydropyranyl derivatives **C2** and **C3**, where the silyl group remained in the ring without any phenyl migration. In all the cases, the Lewis acid counterion (TMSO, chloride or bromide) was effectively incorporated in the final heterocycle [20]. All cyclization reactions proceeded with good yields and excellent stereo-control, resulting in the formation of a single diastereoisomer in each case. The versatility of this methodology is remarkable, since it allows the synthesis of structurally diverse substrates from common intermediates (vinylsilyl alcohol **2** and bromopiperonal), by varying the nature of the catalyst employed.

The UV spectra of the three compounds (Fig. S1) showed maxima at 295 nm, with molar extinction coefficients of $6.5 \pm 0.2\ \mu M^{-1}\ cm^{-1}$ (**C1**), $3.03 \pm 0.03\ \mu M^{-1}\ cm^{-1}$ (**C2**) and $4.545 \pm 0.006\ \mu M^{-1}\ cm^{-1}$ (**C3**).

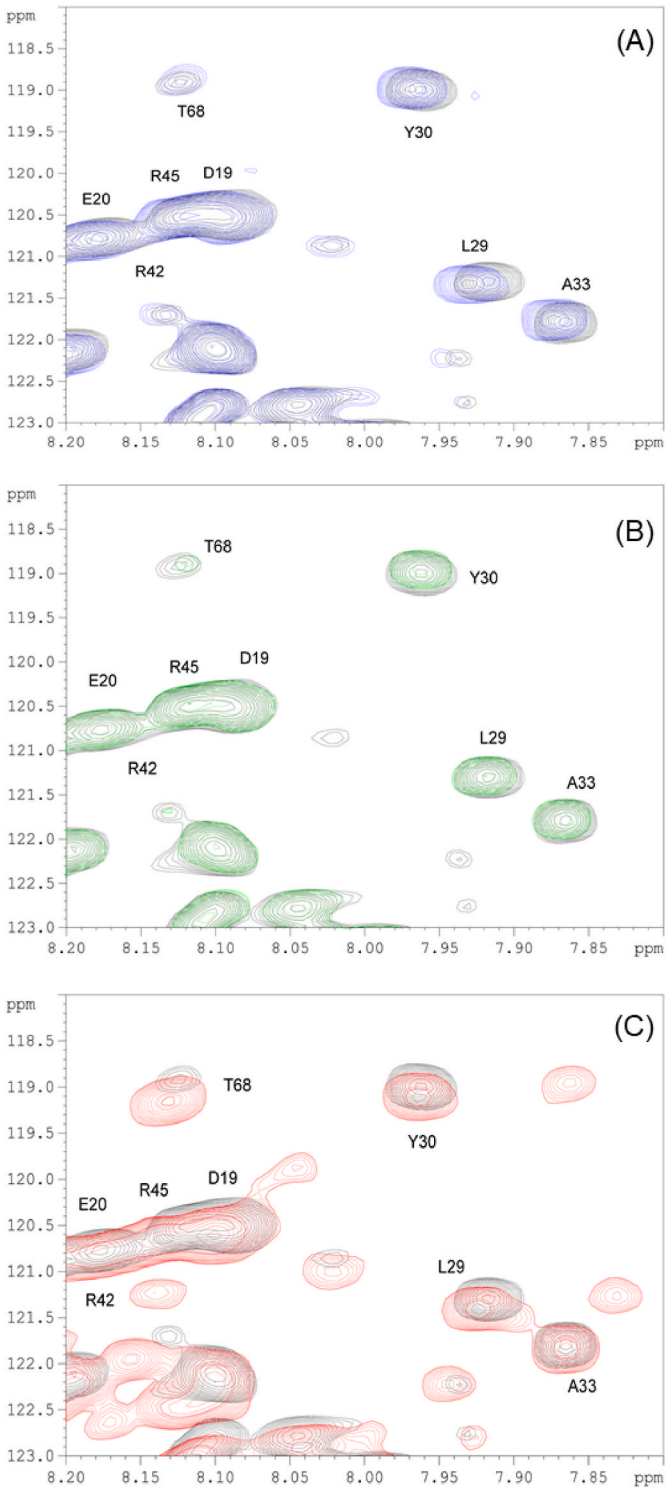

Fig. 2. Binding of the silyl compounds to NUPR1 monitored by NMR: Selected regions of the 2D ^{1}H, ^{15}N-HSQC spectra of NUPR1 in the presence of the silyl compounds: **C1** (blue) (A); **C2** (green) (B); and **C3** (red) (C); in all panels, the spectrum of isolated NUPR1 (in the presence of 0.4 % (v/v) of DMSO) is shown in black. The spectra in each panel were drawn with the same lower contour level. Experiments were carried out at 25 °C. (For interpretation of the references to color in this figure legend, the reader is referred to the Web version of this article.)

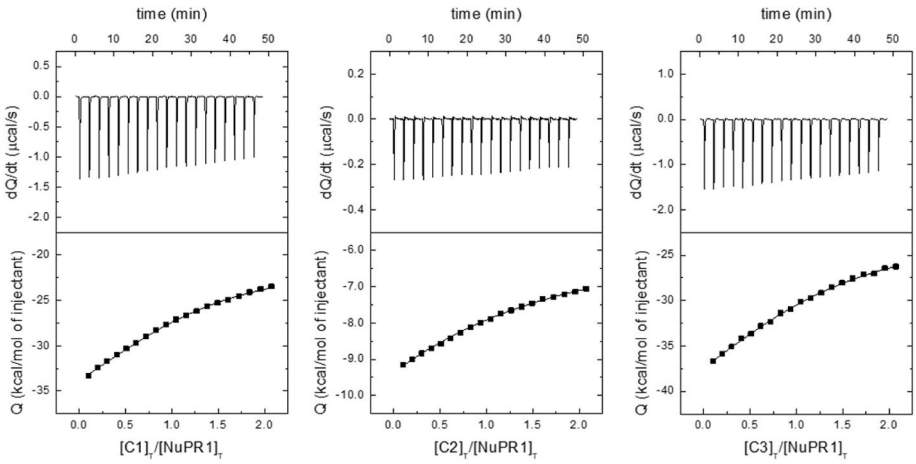

Fig. 3. Binding of the silyl compounds to NUPR1 monitored by ITC: Calorimetric titrations for NUPR1 binding to **C1** (left side), **C2** (middle) and **C3** (right). Upper panels show the thermograms (thermal power as a function of time), and lower panels show the binding isotherms (ligand-normalized heat effects per injection, as a function of the molar ratio in the calorimetric cell). Continuous lines correspond to the fitting curves according to a single-ligand binding site interaction model.

3.2. NUPR1 was bound to the organosilicon compounds with low micromolar affinity

We tested the binding of the organosilicon compounds by using several biophysical and spectroscopic techniques. First, we used bi-dimensional NMR spectroscopy to determine whether there was binding between NUPR1 and the organosilicon compounds, which could lead to changes in chemical shifts and/or signal intensity of the cross-peaks of residues. And second, to determine quantitatively the strength of the binding, we measured the affinity of the silyl compound towards NUPR1 by using ITC and BLI.

3.2.1. NMR spectroscopy

We acquired 2D ^{1}H, ^{15}N-HSQC spectra of isolated NUPR1 (with a final 0.4 % (v/v) DMSO), and in the presence of an excess of each of the three different silyl compounds. [11,13,29]. To this aim, 2D ^{1}H,^{15}N-HSQC NMR experiments were carried out with ^{15}N-labeled NUPR1. In isolation or in the presence of any of the compounds, NUPR1 remained disordered, as indicated by: (i) the clustering of signals in the 2D ^{1}H,^{15}N-HSQC spectra of NUPR1 (Fig. S3 and S4); and (ii) the lack of changes in chemical shifts of the cross-peaks of residues such as Asp19 or Arg45 (Fig. 2). However, in contrast to what happens with other small drugs explored within the same range of concentrations, where only changes in broadening of cross-peaks occurs [11,13,26], the organosilicon compounds caused changes in chemical shifts of different cross-peaks located in the hot-spot regions of NUPR1 (Fig. 2, S2 and S3). Furthermore, in the case of **C3**, new signals appeared (Fig. 2C); in fact, the spectrum in the presence of **C3** showed the largest changes in chemical shifts, when compared to those of **C1** and **C2**. These additional peaks could be due to slow conformational exchange of several residues or to the displacement of the cross-peaks of particular amino acids upon **Ci** addition. On the other hand, the spectrum of NUPR1 in the presence of **C2** showed the smallest changes in chemical shifts, when compared to that of isolated NUPR1 (Fig. 2 B); in fact, changes in the spectrum of NUPR1 in the presence of this compound only occurred in the broadening of some cross-peaks. The absence of large changes in chemical shifts, in the presence of the silyl compounds, suggests that NUPR1 was bound in a fuzzy configuration ensemble, as it happens when it interacts with other drugs [11,13,26].

Therefore, we can conclude that the three silyl compounds were bound to the two hot-spots of NUPR1.

Table 1
Affinity (equilibrium) measurements of the organosilicon compounds to NUPR1, as determined by ITC (at 25 °C).

	ITC[a]			
Silyl compound	K_a (M^{-1})	K_d (µM)	Δ*H* (kcal/mol)	n
C1	6.7×10^4	15	−21	1.1
C2	8.3×10^4	12	−11	1.1
C3	5.6×10^4	18	−27	1.2

[a] Uncertainties are from fitting to the binding isotherm. Errors are estimated to be 10 % of the indicated value.

3.2.2. ITC

ITC is the current gold standard to determine the thermodynamic parameters of a binding reaction. It has been already used with success as one of the main techniques in our previous screening campaigns targeting NUPR1 with other drugs [11,13,26]. The calorimetric titrations of the three silyl compounds provided binding isotherms compatible with moderate-to-low affinity (K_d in the range 10–20 µM). The presence of a considerable percentage of DMSO (17 %) did not prevent binding, but caused a large background injection heat that was properly accounted for in the data analysis.

The binding of the compounds was enthalpically driven, with a large entropic penalty (Fig. 3 and Table 1). In all cases, a 1:1 binding stoichiometry was obtained between the protein and each of the silyl compounds. This is equivalent to the presence of a single binding site for the compounds anchored to NUPR1, although the disordered nature of NUPR1 in the association with any of its molecular partners [5,7,21] suggests that it should correspond to a fuzzy binding pocket.

Table 2
Kinetic parameters of the binding reactions of the organosilicon compounds with NUPR1 (at 25 °C).

Silyl compound	k_{on} (µM^{-1} s^{-1})[a]	k_{off} (s^{-1})[a]	K_d (µM) (= k_{off}/k_{on})[b]
C1	0.006 ± 0.002	-[c]	-[c]
C2	0.00028 ± 0.00007	0.004 ± 0.002	14 ± 7
C3	0.0019 ± 0.0003	0.049 ± 0.007	26 ± 10

[a] Uncertainties are from fitting to Eq. (4).
[b] Uncertainties are calculated as propagation errors.
[c] Not determined because the y-axis intercept of the pseudo-first order line (Eq. (5)) was negative.

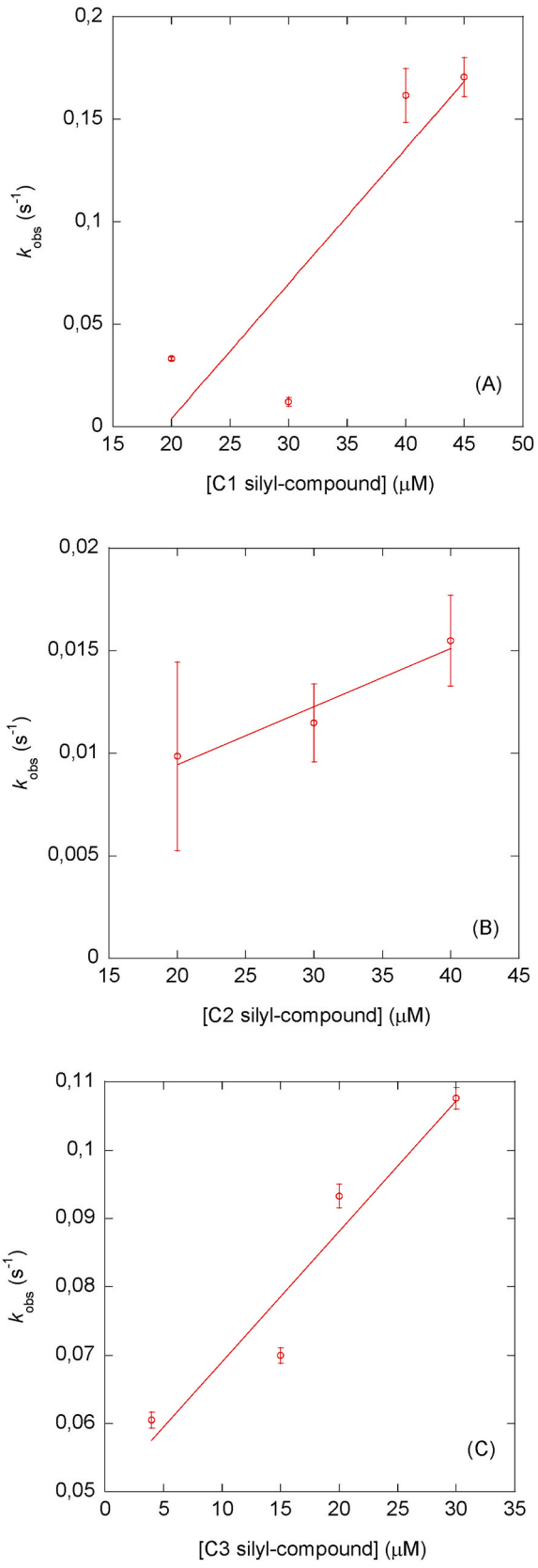

Fig. 4. Binding of the silyl compounds to NUPR1 monitored by BLI: Pseudo-first order plots for **C1**(A), **C2** (B) and **C3** (C). The uncertainties shown are those corresponding to the fitting of sensorgrams to Eq. (3) to obtain the k_{obs} (s^{-1}). Experiments were carried out at 25 °C.

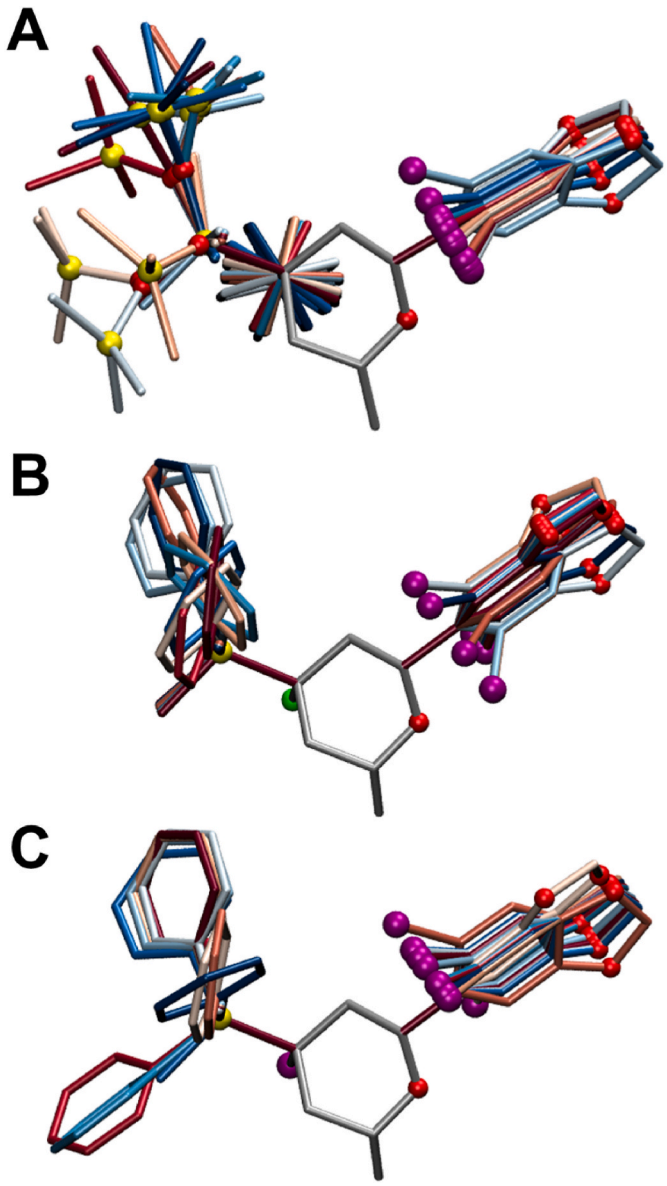

Fig. 5. Preferred conformations of the silyl compounds bound to the hot-spot regions of NUPR1: (A) Compound **C1**; (B) compound **C2**; and (C) compound **C3**. The structures correspond to the ten most favorable docking poses obtained in simulation, with the hot-spot regions $S^{31}LAHS^{35}$ and $L^{66}VTKL^{70}$ omitted for clarity. The conformations are superimposed by fixing the position of the central ring (gray), and colored according to decreasing docking score (color gradient from red to blue). Non-carbon atoms are explicitly shown (spheres). (For interpretation of the references to color in this figure legend, the reader is referred to the Web version of this article.)

3.2.3. BLI

To complement the results obtained by ITC, we also employed BLI, which is a sensitive, label-free technique, to assess interactions between biomolecules. The sensorgrams obtained (Fig. S4) were fitted to Eq. (4) for each of the concentrations used for the organosilicon compounds (in the range 4–45 μM). The k_{on} rates varied by an order of magnitude among the three silyl compounds, as the k_{off} rates did as well (Table 2, Fig. 4). The compound with the slowest k_{on} rate was **C2**, possibly due to the smaller volume of the Cl atom, when compared to that of Br in **C3**. We also observed that **C3** had an intermediate value of the k_{on} rate compared to the other two compounds, and differences with respect to **C1** were probably due to the larger volume of its phenyl group compared to the octadecyltrimethoxysilane (OTMS) moiety of the latter. The

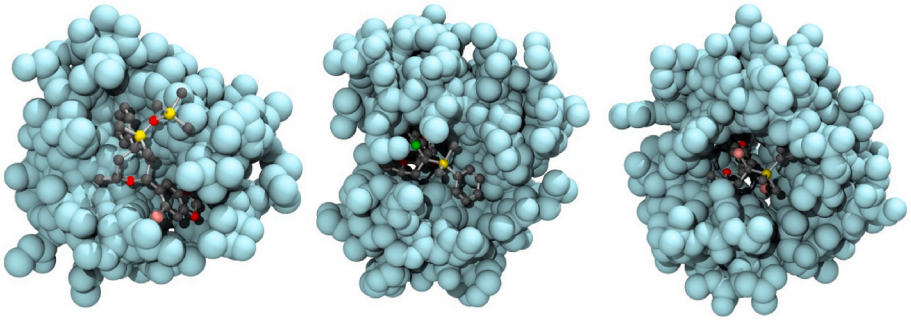

Fig. 6. Preferred distribution of the atoms of the two hot-spot regions around the silyl compounds: (A) **C1**; (B) **C2**; and (C) **C3**. The fuzzy 'cloud' (cyan) corresponds to non-hydrogen atoms of the ten most favorable docking poses obtained in simulation for the hot-spot regions $S^{31}LAHS^{35}$ and $L^{66}VTKL^{70}$, with a single representative binding mode of each silyl compound shown for clarity. (For interpretation of the references to color in this figure legend, the reader is referred to the Web version of this article.)

affinity constants, K_d, obtained assuming a two-state process, were similar to those obtained by ITC (Table 1).

3.3. The organosilicon compounds clamped the hot-spots of NUPR1

The most common hot-spots of NUPR1 for the interaction with other molecular partners are the two short sequence regions located around Ala33 and Thr68, each including a few (usually 5–7) consecutive protein residues [11,30]. Since these two regions are the same identified here also for our silyl compounds (Fig. 2), we followed a protocol previously adopted to model the interaction of NUPR1 with other drug-like molecules [12,13,26]. This methodology consists in using fully-flexible molecular docking to simulate each compound bound to the two 5-residues hot-spot regions $S^{31}LAHS^{35}$ and $L^{66}VTKL^{70}$.

The results reported in Fig. 5 show the conformations spanned by the sole silyl compounds in the ten most favorable docking poses obtained in simulation (with the hot-spot regions $S^{31}LAHS^{35}$ and $L^{66}VTKL^{70}$ omitted for clarity). Each ligand assumed a bent (as opposed to extended) conformation, with the central oxane ring acting as a pivot, while the other outermost regions of the compounds tended to form a clamp to interact with the NUPR1 fragments. The two hot-spot regions of NUPR1 in simulations were consistently found placed inside or around the jaws of this sort of 'molecular plier' (an example is reported in Fig. S5). This effect is clearly visible in Fig. 6, which is complementary to Fig. 6, as it displays the distribution of atoms of the sole NUPR1 hot-spot regions, for the ten most favorable docking poses obtained in simulation (with a single representative binding mode of each silyl compound shown for clarity). The fuzzy 'cloud' constituted by the two hot-spot regions of NUPR1 surrounds each of the three compounds on only one side, forming a transient binding cavity of the protein.

These results suggest that the binding of the organosilicon compounds is driven by heterogeneous interactions, as it is typical for highly disordered proteins [31]. In this specific case, they include not only electrostatic and polar interactions, which are usually dominant in IDPs, but also apolar type. This observation agrees with the fact that the two hot-spot fragments $S^{31}LAHS^{35}$ and $L^{66}VTKL^{70}$ are the ones with the largest relative hydropathy score along the sequence of NUPR1 [11].

3.4. The organosilicon molecules did not show any inhibitory effect on NUPR1 in cellulo

The cytotoxic effect of pharmacological NUPR1 inhibitors has been widely described in the literature [26]. However, none of the inhibitors reported so far were silicon-based. Therefore, we tested whether our silyl compounds could exert any cytotoxic effect on the pancreatic cancer cell line MiaPaCa. We could only detect a slight decrease in the cell viability at the higher concentrations tested (Fig. 7 A). Nevertheless, the effects tested were mild, and likely insufficient to perform any relevant biological activity.

As NUPR1 inhibitors with low cytotoxic effects have been previously described [32], we wondered whether the organosilicon compounds could at least impact on the ability of NUPR1 to interact with some of its protein partners. We decided to test the ability of the compounds to hamper the interaction of NUPR1 with Ras-GTPase-activating protein (SH3 domain)-binding protein, G3BP, a well-known cytosolic partner [33], that could be used as a model to test PPIs of NUPR1. Nevertheless, even in this case, we could not detect any changes in the number of dots (indicating specific NUPR1/G3BP interaction) under treatment with the organosilicon compounds (Fig. 7 B), suggesting the absence of any strong biological activity of these molecules.

4. Discussion

In this work, we have synthesized different organosilicon compounds by increasing the bulkiness of the substituents around the central atom of silicon, and we have tested their binding abilities to interact *in vitro* with NUPR1, an IDP that intervenes in PDAC. At the best of our knowledge, this is the first time that organosilicons are being used to target an IDP, enlarging the variety in the chemical space of compounds potentially active against these proteins considered 'undruggable' until very recently. Our results *in vitro* and *in silico* indicate that all the compounds were capable of binding to NUPR1, a protein notoriously challenging to target with drug-like compounds [11].

We have also demonstrated that the organosilicon compounds target the same hot-spots that NUPR1 uses to bind other proteins and DNA [5,7,21]. These hot-spots are centered around residues Ala33 and Thr68, as identified by our NMR spectra, and correspond to the regions where the local hydrophobicity of the protein sequence is relatively higher in an otherwise highly hydrophilic polypeptide chain [11]. The molecular simulations also clarified that the interactions between the silyl compounds and the hot-spot regions of NUPR1 had the tendency to form a transient and highly disordered cavity of the protein where, nevertheless, they were bound with distinct conformational preferences that are common among the three compounds. According to the findings of our ITC experiments, the binding resulted in a well-defined binding stoichiometry, with enthalpic interactions playing a dominant role to drive the association. These overall results are a proof-of-concept that organosilicons can be designed to target IDPs, and provide some well-defined indications on how to improve their binding affinity by a tailored molecular optimization of their structure.

It could be thought that the absence of large changes in the spectra of NUPR1 upon addition of organosilicon compounds is due to the unspecific and weak binding. We have previously shown that when NUPR1 binds to: (i) any biomolecule, such as proteins or DNA [4,5,7,21,34,35]; (ii) large synthetic molecules, such as dendrimers [30]; or (iii) drugs and small peptides [11–13,26,32] the cross-peaks of NUPR1 in the 2D

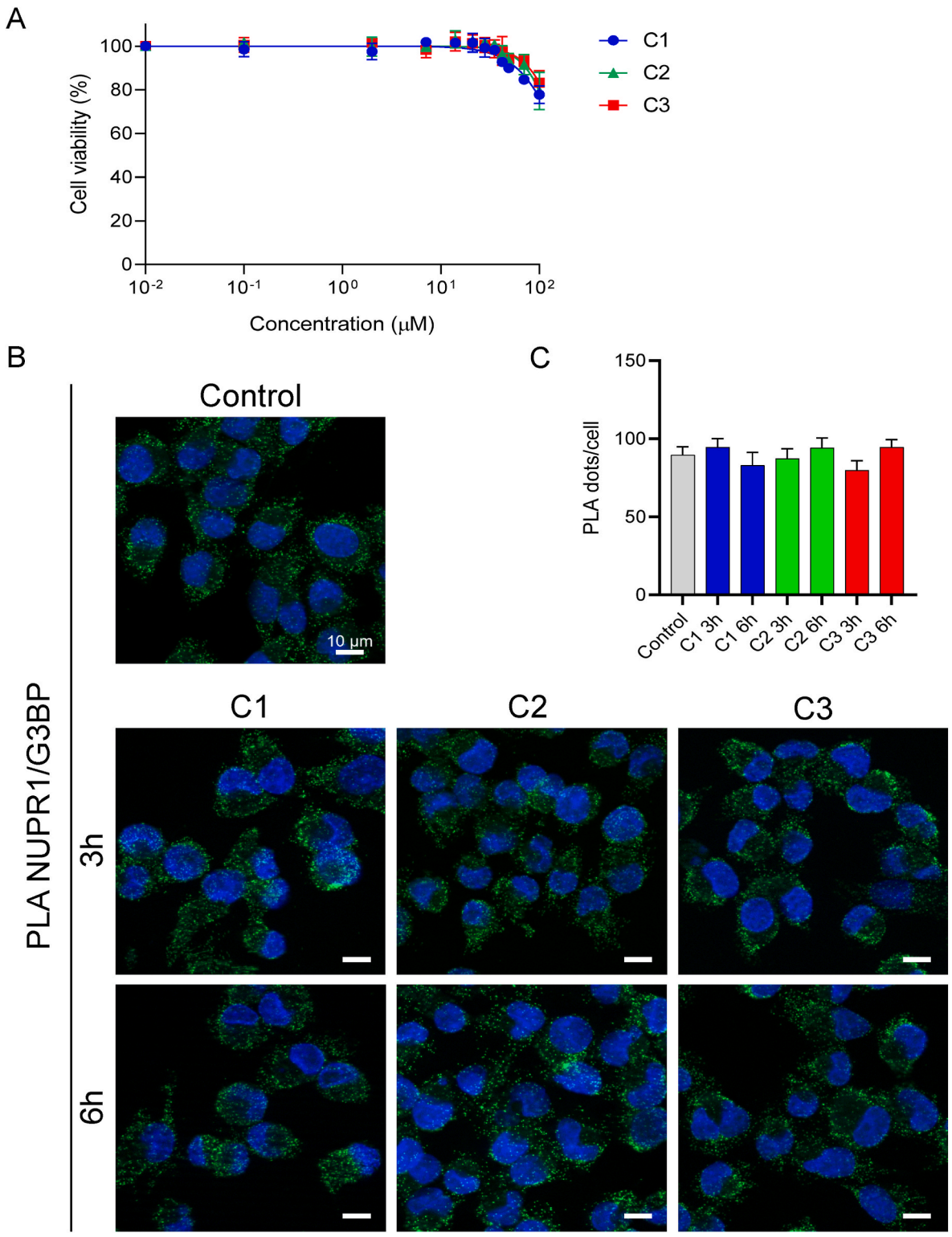

Fig. 7. Evaluation of the effect of the organosilicon molecules as NUPR1 inhibitors *in cellulo*: (A) Cell viability assessed by using the PrestoBlue Reagent assay, after MiaPaCa cells were incubated with the organosilicon molecules for 72 h. The values represent the fraction of cell viability normalized to untreated cells. Data are presented as mean ± standard error of the mean, n = 3 (with duplicates). (B) Interaction with G3BP, a model cytosolic partner of NUPR1 for PPIs, evaluated by using a PLA after MiaPaCa cells were treated with 100 μM of each organosilicon molecule for 6 h. Each panel shows a representative image of the treatment effect. (C) Quantification of the number of dots in each of the compounds at the two times (3 and 6 h) explored for each compound. The bar represents the standard error of the mean.

^{1}H–^{15}N HSQC NMR spectra do not show, in most of the cases, changes in chemical shifts, but rather a peak broadening of selected residues. In only two examples of NUPR1 bound to proteins [21,34], large changes of chemical shifts for some cross-peaks and in broadening of others in the 2D ^{1}H–^{15}N HSQC spectra of NUPR1 were observed. Therefore, the absence of large changes in the chemical shifts of cross-peaks in the NMR

spectra of NUPR1 upon addition of potential partners does not invalidate the occurrence of specific and real binding, as it has also been described in other proteins in DisProt [36]. This absence of large changes in the chemical shifts of cross-peaks in the spectra of NUPR1 with the **Ci** compounds just indicates that the protein remained disordered (fuzzy) upon complex formation.

The affinity constants measured for the silyl compounds were in the 10–20 μM range, which were less favorable than those measured for other drugs targeting NUPR1 [11,13,26]. Furthermore, the binding constants were less favorable even compared with those measured for the natural biological partners of NUPR1, including DNA and other proteins (5–15 μM) [5,7,21]. Noteworthy, it seems that there was no direct relationship between the size of the compound (due to the different substituents added to the silicon) and the affinity constant for NUPR1. We suspect that the relatively low affinity of the organosilicon compounds could preclude the disruption of PPIs of NUPR1 *in cellulo*, resulting in negative PLAs (Fig. 7), when monitoring the possibility of formation of the complex. Under this hypothesis, we suggest that for newly designed drugs against NUPR1, to be effective *in cellulo*, the affinities observed *in vitro* must exceed a certain threshold, and be more favorable than the affinity of NUPR1 for most of its protein partners. This value, in the case of NUPR1, appears to be close to 10 μM [11,13,28]. Affinity dissociation constants less favorable than this threshold value will result in a lack of activity *in cellulo*, because the compounds are not capable of inhibiting the PPIs occurring in the cellular milieu. However, it is important to stress out that, as shown in some compounds targeting other proteins [13,37], lack of functional activity does not result always from a weaker affinity. Whatever the exact reason behind the lack of functional activity of the organosilicon compounds, our study on the use of these molecules against an IDP opens the door to further develop molecules of this type to improve the affinity against NUPR1.

Another important question is whether our compounds can enter the cells to exert their inhibitory function. Although their affinity constant for NUPR1 is moderate, we do not know the exact reasons why they did not show any detectable activity *in cellulo* (as demonstrated by using either PLA or cell viability assays). In fact, other examples of bulkier organosilicons have showed a larger activity *in cellulo* against a variety of protein targets (see Ref. [18] and references therein). On the other hand, the relatively high hydrophobicity of our organosilicon compounds, which also plays a role in the binding to NUPR1 as observed in our molecular docking simulations, could hamper their entry into the cell through the cell membrane. In fact, it has been suggested that organosilicon compounds could be retained at the membrane cell [38]. We have observed a similar effect previously in the design of amphipathic helical peptides capable of binding to NUPR1 *in vitro*, but not being capable of crossing the membrane, unless a positive charge in the form of an arginine residue is introduced in their sequences [32]. In the case of the organosilicon compounds, in future studies, we plan to use vehiculation devices (for instance, vesicles or dendrimers) to surmount the crossing of the cell membrane.

5. Conclusion

To sum up, this study pioneers the use of organosilicon compounds against an IDP, further extending the space of potential biologically active molecules against these 'undruggable' proteins. It opens the door to develop novel compounds with improved affinity against NUPR1, which is a validated pharmacological target for PDAC, as well as for other cancers. The binding constants observed for these compounds was enough to achieve protein inhibition *in vitro*, which is already an encouraging success because these compounds were not explicitly designed to bind this difficult target. Moreover, although no significant biological action was observed *in cellulo*, a comparison with other more successful cases provided indications that the affinity of these silyl compounds is already close to the threshold expected to obtain a biological effect. Improvements could be expected by optimizing the affinity towards the hot-spot regions of NUPR1, while possibly reducing the hydrophobicity of the silyl compounds to increase cell penetration. Since a molecular mechanism of binding of these compounds was also modeled, we expect further advances in the drug design of silicon-based compounds against this protein, and envision the possibility to extend similar studies to other IDPs.

CRediT authorship contribution statement

Laura F. Peña: Writing – review & editing, Investigation, Formal analysis. **Matías Estaras:** Writing – review & editing, Writing – original draft, Investigation, Formal analysis, Conceptualization. **Paula González-Andrés:** Writing – review & editing, Investigation, Formal analysis. **Carlos Díez-Poza:** Writing – review & editing, Investigation, Formal analysis. **Bruno Rizzuti:** Writing – review & editing, Writing – original draft, Methodology, Investigation, Formal analysis, Conceptualization. **Olga Abian:** Writing – review & editing, Methodology, Investigation, Formal analysis. **Adrian Velazquez-Campoy:** Writing – review & editing, Writing – original draft, Methodology, Investigation, Funding acquisition, Formal analysis, Conceptualization. **Juan L. Iovanna:** Writing – review & editing, Methodology, Funding acquisition. **Patricia Santofimia-Castaño:** Writing – review & editing, Writing – original draft, Methodology, Investigation, Formal analysis. **José L. Neira:** Writing – review & editing, Writing – original draft, Project administration, Methodology, Investigation, Funding acquisition, Formal analysis, Conceptualization. **Asunción Barbero:** Writing – review & editing, Writing – original draft, Methodology, Funding acquisition, Conceptualization.

Acknowledgements

This research was funded by Ministerio de Ciencia e Innovación MICIN/AEI/10.13039/501100011033/and "ERDF A way of Making Europe" [PID2021-127296OB-I00 to AVC.]; Comunidad Valenciana [CIAICO 2021/0135 to JLN and AVC]; by European Union [EXPLORA GA nº 101181841 to JLN]; by Instituto de Salud Carlos III co-funded by European Social Fund "Investing in your future" [PI18/00394 to OA]; Gobierno de Aragón [Protein Targets and Bioactive Compounds Group E45_23R to AVC, and "Digestive Pathology Group" B25_23R to OA]; La Ligue Contre le Cancer to JLI; INCa 2020-098 to JLI; Fondation ARC to PSC; Ministerio de Ciencia, Innovación y Universidades MICIU/AEI/10.13039/501100011033 and the European Union NextGenerationEU/PRTR [TED2021-131705B–C21 to AB]; LFP and PGA acknowledge predoctoral fellowships funded by the "Junta de Castilla y León" and the University of Valladolid, respectively; ME was the recipient of a postdoctoral fellow from ARC Foundation. BR acknowledges the use of the distributed laboratory of molecular modeling funded by Next Generation EU program, Italian PNNR, Mission 4, Component 2, Investment 1.5, "Innovation Ecosystems" project Tech4You, "Technologies for Climate Change Adaptation and Quality of Life Improvement" (CUP B83C22003980006), Spoke 3.

The funders had no role in the study design, data collection and analysis, decision to publish, or preparation of the manuscript.

We thank the three reviewers for their comments and suggestions. We thank Prof. Pablo Sobrado for handling the manuscript.

Materials are available from the authors upon reasonable request.

Appendix A. Supplementary data

Supplementary data to this article can be found online at https://doi.org/10.1016/j.abb.2025.110513.

Data availability

Data will be made available on request.

References

[1] C.E. Cano, T. Hamidi, M.J. Sandi, J.L. Iovanna, Nupr1: the Swiss-knife of cancer, J. Cell. Physiol. 226 (2011) 1439–1443, https://doi.org/10.1002/JCP.22324.

[2] S. Goruppi, J.L. Iovanna, Stress-inducible protein p8 is involved in several physiological and pathological processes, J. Biol. Chem. 285 (2010) 1577–1581, https://doi.org/10.1074/JBC.R109.080887.

[3] P. Santofimia-Castaño, B. Rizzuti, Y. Xia, O. Abian, L. Peng, A. Velázquez-Campoy, J.L. Neira, J. Iovanna, Targeting intrinsically disordered proteins involved in cancer, Cell. Mol. Life Sci. 77 (2020) 1695–1707, https://doi.org/10.1007/S00018-019-03347-3.

[4] J.A. Encinar, G.V. Mallo, C. Mizyrycki, L. Giono, J.M. González-Ros, M. Rico, E. Cánepa, S. Moreno, J.L. Neira, J.L. Iovanna, Human p8 is a HMG-I/Y-like protein with DNA binding activity enhanced by phosphorylation, J. Biol. Chem. 276 (2001) 2742–2751, https://doi.org/10.1074/JBC.M008594200.

[5] D. Aguado-Llera, T. Hamidi, R. Doménech, D. Pantoja-Uceda, M. Gironella, J. Santoro, A. Velázquez-Campoy, J.L. Neira, J.L. Iovanna, Deciphering the binding between Nupr1 and MSL1 and their DNA-Repairing activity, PLoS One 8 (2013), https://doi.org/10.1371/journal.pone.0078101.

[6] J.L. Neira, B. Rizzuti, A. Jiménez-Alesanco, M. Palomino-Schätzlein, O. Abián, A. Velázquez-Campoy, J.L. Iovanna, A phosphorylation-induced switch in the nuclear localization sequence of the intrinsically disordered NUPR1 hampers binding to importin, Biomolecules 10 (2020) 1–22, https://doi.org/10.3390/BIOM10091313.

[7] P. Santofimia-Castaño, B. Rizzuti, Á.L. Pey, P. Soubeyran, M. Vidal, R. Urrutia, J. L. Iovanna, J.L. Neira, Intrinsically disordered chromatin protein NUPR1 binds to the C-terminal region of polycomb RING1B, Proc. Natl. Acad. Sci. U. S. A. 114 (2017) E6332–E6341, https://doi.org/10.1073/PNAS.1619932114/SUPPL_FILE/PNAS.201619932SI.PDF.

[8] G.V. Mallo, F. Fiedler, E.L. Calvo, E.M. Ortiz, S. Vasseur, V. Keim, J. Morisset, J. L. Iovanna, Cloning and expression of the rat p8 cDNA, a new gene activated in pancreas during the acute phase of pancreatitis, pancreatic development, and regeneration, and which promotes cellular growth, J. Biol. Chem. 272 (1997) 32360–32369, https://doi.org/10.1074/jbc.272.51.32360.

[9] S.B. Su, Y. Motoo, J.L. Iovanna, M.J. Xie, H. Mouri, K. Ohtsubo, Y. Yamaguchi, H. Watanabe, T. Okai, F. Matsubara, N. Sawabu, Expression of p8 in human pancreatic cancer, Clin. Cancer Res. 7 (2001) 309–313.

[10] M.J. Sandi, T. Hamidi, C. Malicet, C. Cano, C. Loncle, A. Pierres, J.C. Dagorn, J. L. Iovanna, p8 expression controls pancreatic cancer cell migration, invasion, adhesion, and tumorigenesis, J. Cell. Physiol. 226 (2011) 3442–3451, https://doi.org/10.1002/JCP.22702.

[11] J.L. Neira, J. Bintz, M. Arruebo, B. Rizzuti, T. Bonacci, S. Vega, A. Lanas, A. Velázquez-Campoy, J.L. Iovanna, O. Abián, Identification of a drug targeting an intrinsically disordered protein involved in pancreatic adenocarcinoma, Sci. Rep. 7 (2017), https://doi.org/10.1038/SREP39732.

[12] B. Rizzuti, W. Lan, P. Santofimia-Castaño, Z. Zhou, A. Velázquez-Campoy, O. Abián, L. Peng, J.L. Neira, Y. Xia, J.L. Iovanna, Design of inhibitors of the intrinsically disordered protein NUPR1: balance between drug affinity and target function, Biomolecules 11 (2021), https://doi.org/10.3390/BIOM11101453.

[13] P. Santofimia-Castaño, Y. Xia, W. Lan, Z. Zhou, C. Huang, L. Peng, P. Soubeyran, A. Velázquez-Campoy, O. Abián, B. Rizzuti, J.L. Neira, J. Iovanna, Ligand-based design identifies a potent NUPR1 inhibitor exerting anticancer activity via necroptosis, J. Clin. Investig. 129 (2019) 2500–2513, https://doi.org/10.1172/JCI127223.

[14] S.Y. Choi, Y.S. Koh, S.H. Jo, Inhibition of human ether-a-go-go-related gene K+ channel and IKr of Guinea pig cardiomyocytes by antipsychotic drug trifluoperazine, J. Pharmacol. Exp. Therapeut. 313 (2005) 888–895, https://doi.org/10.1124/JPET.104.080853.

[15] G.W. Bemis, M.A. Murcko, The properties of known drugs. 1. Molecular frameworks, J. Med. Chem. 39 (1996) 2887–2893, https://doi.org/10.1021/JM9602928.

[16] G.W. Bemis, M.A. Murcko, Properties of known drugs. 2. Side chains, J. Med. Chem. 42 (1999) 5095–5099, https://doi.org/10.1021/JM9903996.

[17] J.S. Mills, G.A. Showell, Exploitation of silicon medicinal chemistry in drug discovery, Expet Opin. Invest. Drugs 13 (2004) 1149–1157, https://doi.org/10.1517/13543784.13.9.1149.

[18] J.L. Panayides, D.L. Riley, F. Hasenmaile, W.A.L. van Otterlo, The role of silicon in drug discovery: a review, RSC Med. Chem. 15 (2024), https://doi.org/10.1039/D4MD00169A.

[19] T.T. Talele, Opportunities for tapping into three-dimensional chemical space through a Quaternary carbon, J. Med. Chem. 63 (2020) 13291–13315, https://doi.org/10.1021/ACS.JMEDCHEM.0C00829/ASSET/IMAGES/MEDIUM/JM0C00829_0047.GIF.

[20] C. Díez-Poza, L. Fernández-Peña, P. González-Andrés, A. Barbero, Changing the reaction pathway of silyl-prins cyclization by switching the lewis acid: application to the synthesis of an antinociceptive compound, J. Org. Chem. 88 (2023) 6776–6783, https://doi.org/10.1021/ACS.JOC.3C00050.

[21] S. Araujo-Abad, J.L. Neira, B. Rizzuti, P. García-Morales, C. de Juan Romero, P. Santofimia-Castaño, J. Iovanna, Intrinsically disordered chromatin protein NUPR1 binds to the enzyme PADI4, J. Mol. Biol. 435 (2023), https://doi.org/10.1016/J.JMB.2023.168033.

[22] S.C. Gill, P.H. von Hippel, Calculation of protein extinction coefficients from amino acid sequence data, Anal. Biochem. 182 (1989) 319–326, https://doi.org/10.1016/0003-2697(89)90602-7.

[23] M. Piotto, V. Saudek, V. Sklenář, Gradient-tailored excitation for single-quantum NMR spectroscopy of aqueous solutions, J. Biomol. NMR 2 (1992) 661–665, https://doi.org/10.1007/BF02192855.

[24] M. Bastos, O. Abian, C.M. Johnson, F. Ferreira da Silva, S. Vega, A. Jiménez-Alesanco, D. Ortega-Alarcón, A. Velazquez-Campoy, Isothermal titration calorimetry, Nature Reviews Methods Primers 3 (2023) 18, https://doi.org/10.1038/s43586-023-00216-z.

[25] D. Frenzel, D. Willbold, Kinetic titration series with biolayer interferometry, PLoS One 9 (2014) e106882, https://doi.org/10.1371/JOURNAL.PONE.0106882.

[26] X. Liu, A. Jimenez-Alesanco, Z. Li, B. Rizzuti, J.L. Neira, M. Estaras, L. Peng, E. Chuluyan, J. Garona, F. Gottardo, A. Velazquez-Campoy, Y. Xia, O. Abian, P. Santofimia-Castaño, J. Iovanna, Development of an efficient NUPR1 inhibitor with anticancer activity, Sci. Rep. 14 (2024), https://doi.org/10.1038/S41598-024-79340-Z.

[27] G.M. Morris, H. Ruth, W. Lindstrom, M.F. Sanner, R.K. Belew, D.S. Goodsell, A. J. Olson, AutoDock4 and AutoDockTools4: automated docking with selective receptor flexibility, J. Comput. Chem. 30 (2009) 2785–2791, https://doi.org/10.1002/JCC.21256.

[28] J. Eberhardt, D. Santos-Martins, A.F. Tillack, S. Forli, AutoDock Vina 1.2.0: new docking methods, expanded force field, and Python bindings, J. Chem. Inf. Model. 61 (2021) 3891–3898, https://doi.org/10.1021/ACS.JCIM.1C00203.

[29] C. Díez-Poza, A. Barbero, Unexpected domino silyl-Prins/Aryl migration process from geminal vinylsilyl alcohols, Org. Lett. 23 (2021) 8385–8389, https://doi.org/10.1021/ACS.ORGLETT.1C03121.

[30] J.L. Neira, J. Correa, B. Rizzuti, P. Santofimia-Castaño, O. Abian, A. Velázquez-Campoy, E. Fernandez-Megia, J.L. Iovanna, Dendrimers as competitors of protein-protein interactions of the intrinsically disordered nuclear chromatin protein NUPR1, Biomacromolecules 20 (2019), https://doi.org/10.1021/acs.biomac.9b00378.

[31] A. Hatos, J.M.C. Teixeira, S. Barrera-Vilarmau, A. Horvath, S.C.E. Tosatto, M. Vendruscolo, M. Fuxreiter, FuzPred: a web server for the sequence-based prediction of the context-dependent binding modes of proteins, Nucleic Acids Res. 51 (2023) W198–W206, https://doi.org/10.1093/NAR/GKAD214.

[32] P. Santofimia-Castaño, B. Rizzuti, O. Abián, A. Velázquez-Campoy, J.L. Iovanna, J. L. Neira, Amphipathic helical peptides hamper protein-protein interactions of the intrinsically disordered chromatin nuclear protein 1 (NUPR1), Biochim. Biophys. Acta Gen. Subj. 1862 (2018) 1283–1295, https://doi.org/10.1016/J.BBAGEN.2018.03.009.

[33] P. Santofimia-Castaño, N. Fraunhoffer, X. Liu, I.F. Bessone, M.P. di Magliano, S. Audebert, L. Camoin, M. Estaras, M. Brenière, M. Modesti, G. Lomberk, R. Urrutia, P. Soubeyran, J.L. Neira, J. Iovanna, Targeting NUPR1-dependent stress granules formation to induce synthetic lethality in KrasG12D-driven tumors, EMBO Mol. Med. 16 (2024) 475–505, https://doi.org/10.1038/S44321-024-00032-2.

[34] P. Santofimia-Castaño, B. Rizzuti, A.L. Pey, M.E. Fárez-Vidal, J.L. Iovanna, J. L. Neira, Intrinsically disordered protein NUPR1 binds to the armadillo-repeat domain of Plakophilin 1, Int. J. Biol. Macromol. 170 (2021) 549–560, https://doi.org/10.1016/J.IJBIOMAC.2020.12.193.

[35] C. Malicet, V. Giroux, S. Vasseur, J.C. Dagorn, J.L. Neira, J.L. Iovanna, Regulation of apoptosis by the p8/prothymosin α complex, Proc. Natl. Acad. Sci. U. S. A. 103 (2006) 2671–2676, https://doi.org/10.1073/PNAS.0508955103/SUPPL_FILE/08955FIG7.PDF.

[36] M.C. Aspromonte, M.V. Nugnes, F. Quaglia, A. Bouharoua, S.C.E. Tosatto, D. Piovesan, V. Sagris, V.J. Promponas, A. Chasapi, E. Fichó, G.E. Balatti, G. Parisi, M.G. Buitrón, G. Erdos, M. Pajkos, Z. Dosztányi, L. Dobson, A. Del Conte, D. Clementel, E. Salladini, E. Leonardi, F. Kordevani, H. Ghafouri, L.G. Tenorio Ku, A.M. Monzon, C. Ferrari, Z. Kálmán, J.F. Nilsson, J. Santos, C. Pintado-Grima, S. Ventura, V. Ács, R. Pancsa, M.G. Kulik, M.A. Andrade-Navarro, P.J.B. Pereira, S. Longhi, P. Le Mercier, J. Bergier, P. Tompa, T. Lazar, DisProt in 2024: improving function annotation of intrinsically disordered proteins, Nucleic Acids Res. 52 (2024) D434–D441, https://doi.org/10.1093/NAR/GKAD928.

[37] L.J. Byrnes, W.Y. Choi, P. Balbo, M.E. Banker, J. Chang, S. Chen, X. Cheng, Y. Cong, J. Culp, H. Di, M. Griffor, J. Hall, X. Meng, B. Morgan, J.J. Mousseau, J. Nicki, T. O'Connell, S. Ramsey, A. Shaginian, S. Shanker, J. Trujillo, J. Wan, F. Vincent, S. W. Wright, F. Vajdos, Discovery, characterization, and structure of a cell active PAD2 inhibitor acting through a novel allosteric mechanism, ACS Chem. Biol. 19 (2024), https://doi.org/10.1021/ACSCHEMBIO.4C00397.

[38] P. Beekman, A. Enciso-Martinez, S.P. Pujari, L.W.M.M. Terstappen, H.T. Zuilhof, S. Le Gac, C. Otto, Organosilicon uptake by biological membranes, Commun. Biol. 4 (2021), https://doi.org/10.1038/S42003-021-02155-5.